

CFD Prediction of Shock Wave Impacting a Cylindrical Water Column

Viola Rossano and Giuliano De Stefano(✉)

Engineering Department, University of Campania Luigi Vanvitelli, 81031 Aversa, Italy
giuliano.destefano@unicampania.it

Abstract. Computational fluid dynamics (CFD) analysis is carried out to evaluate the early stages of the aerobreakup of a cylindrical water column due to the impact of a travelling plane shock wave. The mean flow in a shock tube is simulated by adopting the compressible unsteady Reynolds-averaged Navier-Stokes modelling approach, where the governing equations are solved by means of a finite volume-based numerical technique. The volume of fluid method is employed to track the transient interface between air and water on the fixed numerical mesh. The present computational modelling approach for industrial gas dynamics applications is verified to have significant practical potential by making a comparison with reference experiments and numerical simulations.

Keywords: Aerobreakup · Computational fluid dynamics · Industrial gas dynamics · Shock tube

1 Introduction

The aerodynamic breakup of liquid droplets impacted by shock waves has a number of important industrial applications including, for instance, supersonic combustion airbreathing jet engines (scramjets), where the behavior of fuel droplets in supersonic airflow plays a crucial role [1,2]. Experimentally, this physical phenomenon can be studied by using a shock tube device, wherein a planar shock wave is produced that travels towards the downstream test section, with uniform gaseous flow conditions being established, e.g. [3,4]. Computationally, the droplet breakup can be approximated in two spatial dimensions by considering a water cylinder with circular section in the high-speed flow behind a travelling shock wave. The latter can be obtained by numerically reproducing the shock tube flow conditions that are given and known.

The main goal of the present work is the computational evaluation of the aerodynamic breakup of a cylindrical water column. The study is focused on the initial stages in the interaction process between the travelling plane shock wave and the water cylinder at relatively high Mach number. In fact, the gas flow Mach number that is Ma = 1.73 corresponds to one of the cases recently studied in [5]. The numerical experiments are conducted by employing one of the CFD solvers

© Springer Nature Switzerland AG 2021
O. Gervasi et al. (Eds.): ICCSA 2021, LNCS 12949, pp. 376–386, 2021.
https://doi.org/10.1007/978-3-030-86653-2_28

that are commonly and successfully used for building virtual wind tunnels in the industrial gas dynamics research, e.g. [6,7]. The compressible unsteady Reynolds-averaged Navier-Stokes (URANS) equations [8], supplied with a suitable closure model, are solved by means of a finite volume-based numerical technique. The transient interface between air and water is approximated on the fixed numerical mesh by using the volume of fluid (VOF) method [9]. The overall computational modelling procedure is validated against reference experimental and numerical data corresponding to the same flow configuration.

In the following, after introducing the main aspects of the present CFD modelling procedure, the results of the numerical simulation are presented and discussed. Finally, some concluding remarks are provided.

2 CFD Model

2.1 Flow Geometry

The simplified two-dimensional geometry of the shock tube device is reproduced by means of a rectangular domain. The coordinates system (x, y), with the x-axis coinciding with the shock tube axis, is chosen so that $-8 < x/D_0 < 15$ and $-10 < y/D_0 < 10$, where D_0 represents the initial diameter of the cylindrical water column. The origin of the system corresponds to the initial position of the leading edge of the column, which is immersed in supersonic air crossflow. The flow configuration is sketched in Fig. 1, where V_1 represents the constant velocity of the travelling planar shock wave.

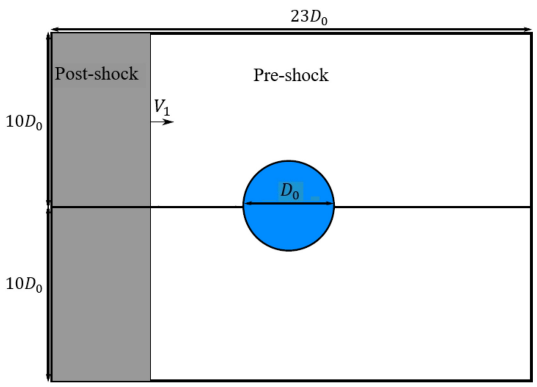

Fig. 1. Sketch of physical domain, with travelling air shock wave.

The shock tube flow conditions are simulated by initially imposing two very different pressure levels into the two different tube sections, separated by a virtual cross diaphragm, which is located upstream of the column at $x/D_0 = -2$. Initially, both tube sections contain still air, which is treated as ideal gas, at the same temperature and very different densities. Given and known the pressure level, say p_1, in the driven section (right side), as well as the compression ratio across the shock, p_2/p_1 (associated to the prescribed Mach number), the pressure level p_4 to be imposed in the driver section (left side), is analytically determined by exploiting the theoretical shock tube relations [10]. As is demonstrated in the next section, the present CFD model is able to reproduce a plane shock wave travelling at the prescribed velocity that is $V_1 = 594$ m/s. For brevity, the flow parameters corresponding to the simulated shock tube device are reported in Table 1.

Table 1. Shock tube parameters.

Parameter	Value
Driven section pressure	$p_1 = 101.3$ kPa
Driven section density	$\rho_1 = 1.204$ kg/m^3
Shock compression ratio	$p_2/p_1 = 3.32$
Driver section pressure	$p_4 = 1.50$ MPa
Driver section density	$\rho_4 = 17.8$ kg/m^3
Temperature	$T_1 = T_4 = 293.15$ K
Travelling shock velocity	$V_1 = 594$ m/s

It is worth noting that the actual computational domain corresponds to half the physical domain sketched in Fig. 1, with a symmetry condition at the centerline ($y = 0$) being imposed. In fact, previous experiments conducted at comparable characteristic flow numbers demonstrated that flow symmetry is maintained in the early stages of the aerobreakup process [11]. Also, wall boundary conditions are set at the other three edges of the computational domain.

For the current flow configuration, the Reynolds and Weber numbers are defined based on the reference length D_0 and the air conditions behind the shock, specifically,

$$\mathrm{Re} = \frac{\rho_2 V_2 D_0}{\mu_2} \ , \qquad \mathrm{We} = \frac{\rho_2 V_2^2 D_0}{\sigma} \ .$$

Given the values for the flow parameters that are reported in Table 2, where the surface tension σ at the interface between air and water is assumed constant, the above characteristic numbers result in being $\mathrm{Re} = 2.38 \times 10^5$ and $\mathrm{We} = 1.93 \times 10^4$. Therefore, based on the present high Weber number, in the early stages of the aerobreakup, capillary effects can be neglected with respect to inertial ones. In fact, according to the recent reclassification of the droplet breakup regimes

Table 2. Water column and post-shock air flow parameters.

Parameter	Value
Initial column diameter	$D_0 = 4.80 \times 10^{-3}$ m
Liquid water density	$\rho_w = 1000$ kg/m^3
Surface tension	$\sigma = 7.286 \times 10^{-2}$ N/m
Air density	$\rho_2 = 2.706$ kg/m^3
Air pressure	$p_2 = 0.336$ M Pa
Air viscosity	$\mu_2 = 1.80 \times 10^{-5}$ Pa s
Air velocity	$V_2 = 329$ m/s
Mach number	$\mathrm{Ma}_2 = 0.789$

proposed in [12], the current flow configuration belongs to the shear-induced entrainment regime, where the gas goes around the liquid mass producing a surface layer peeling-and-ejection action [13]. Finally, differently from what done in [5], the viscous effects are not ignored in the present study.

2.2 VOF Method

To approximate the transient interface between the gas (air) and the liquid (water), while tracking it on the fixed numerical mesh, a classical methodology that is based on the concept of fractional volume of fluid is used. This technique was shown to be more flexible and efficient for treating the complex interface between two immiscible fluids, when compared to other methods [9]. Following the VOF approach, the same governing equations are solved for the two different fluid phases, while assuming that they share the velocity, pressure and temperature fields. Practically, the balance equations are solved for an effective fluid, whose averaged properties are evaluated according to the two volume fractions. For instance, the averaged density is defined as

$$\rho = \alpha\rho_w + (1 - \alpha)\rho_a,$$

where ρ_a stands for the air density, and α represents the volume fraction of water. The latter variable is calculated throughout the computational domain by solving the associated continuity equation.

2.3 CFD Solver

The shock tube flow, along with the aerodynamic breakup of the water column, is numerically predicted by solving the URANS equations, which describe the unsteady mean turbulent compressible flow. The governing equations are supplied with the k–ω SST two-equation turbulence model [14]. The resolved compressible URANS equations, which are not reported here for brevity, can be found, for instance, in [8].

The current numerical simulations are performed by means of the industrial solver ANSYS Fluent 19, which has been successfully employed by the authors in previous industrial CFD studies using Reynolds-averaging based models, e.g. [15–17]. The pressure-based solver utilizes the Finite Volume (FV) method to approximate the mean flow solution, with the conservation principles being applied over each control volume, e.g. [18]. The results presented in the following have been obtained using a mesh consisting of about 2.8×10^5 FV cells. The mesh has been suitably refined in the space region close to the position of the water column, including the near wake, where the numerical resolution corresponds to about 50 cells per cylinder diameter. The constant time-step size $\Delta t = 1$ μs has been used for the explicit transient calculation.

3 Results

The shock tube flow is simulated starting from the initial conditions discussed in the previous section. Specifically, a planar shock wave develops and travels towards the driven section, where the water column is located, while a set of expansion waves propagate in the opposite direction, towards the driver section. The robustness of the CFD model and the accuracy of the time-dependent solution have been assessed through comparison with the analytical ideal shock-tube theory [10]. For instance, the instantaneous pressure profile along the tube at the moment when the incident shock impacts on the column, say $t = t_0$, is reported in Fig. 2. Note that, at the contact surface, which travels in the same direction of the shock, though at lower velocity, it holds $p_3 = p_2$, whereas $\rho_3 > \rho_2$.

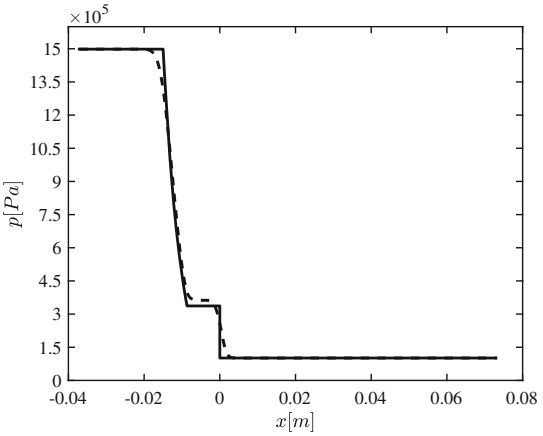

Fig. 2. Pressure profile along the shock tube at the impact time instant: present CFD solution (dashed line) compared to theoretical profile (solid line).

As a consequence of the impact of the air shock wave, the deformation and the breakup of the water column are observed. In the following, as is usually

done in droplet aerobreakup studies, the independent time variable is non-dimensionalized as follows

$$t^* = \frac{V_2}{D_0}\sqrt{\frac{\rho_2}{\rho_w}}\,(t - t_0),$$

where ρ_2 and V_2 represent post-shock air flow conditions, corresponding to the Mach number $\mathrm{Ma}_2 = 0.789$ in the shock-moving reference frame.

In the early stages of the interaction process, the water cylinder is flattened in the streamwise direction, which corresponds to a decreasing centerline width, together with an increasing cross-stream length. The initial deformation of the water column is illustrated in Fig. 3, where the contour maps of density (left side) and pressure (right side) are reported at different time instants between $t^* = 0.008$ (top) and 0.72 (bottom). By inspection of this figure, in the very early stage, the air flow field resembles the flow past a circular cylinder. Then, the streamwise flattening of the liquid column is observed, with the successive formation of peripheral tips. Note that, due to the finite numerical resolution, the interface between the two different fluids appears to be diffuse. In Fig. 4, the density and pressure contours are shown at later time instants, namely, between $t^* = 0.96$ (top) and 1.4 (bottom). Apparently, the liquid sheet becomes thinner and thinner until, finally, the rupture indicates the breakup initiation. Then, the water body is continuously eroded at the periphery, with the appearance of microdroplets stripped from the parent column. During the successive stage, the water column would disintegrate into fragments distributed widely in the flow field. These pictures confirm the qualitative features of the so-called shear stripping breakup mechanism, as is expected at current high Weber number [13].

From a quantitative point of view, the present CFD solution is validated against the corresponding numerical solution of Meng and Colonius [5], as well as the experimental findings of Igra and Takayama [11]. Here, the deformed column shape is evaluated as that corresponding to the isoline $\alpha = 0.5$ for the volume fraction of water. The time-dependent centerline width of the deforming water column, say w, is shown in Fig. 5 (left side). Apparently, a good agreement is observed with respect to both numerical and experimental reference data. Note that the two different lines that are reported for the reference numerical solution correspond to $\alpha = 0.25$ (dashed line) and 0.99 (dashed-dotted line). When examining the time-dependent cross-stream length of the column, say d, which is drawn in the same Fig. 5 (right side), the current CFD result, while matching the reference numerical data, appears to be overestimated with respect to experiments. Similarly, a good agreement with reference data is found for the time-dependent section area of the coherent water body, which is shown in Fig. 6 (left side), where A_0 stands for the initial circular section area. When examining the time-dependent position of the water column leading-edge, say Δx, which is reported in the same Fig. 6 (right side), again, the CFD result appears to be overestimated with respect to the experimental findings, while agreeing with the reference numerical data. For a more detailed discussion of the performance of the proposed computational model, the reader is referred to [19], where a more comprehensive study has been completed.

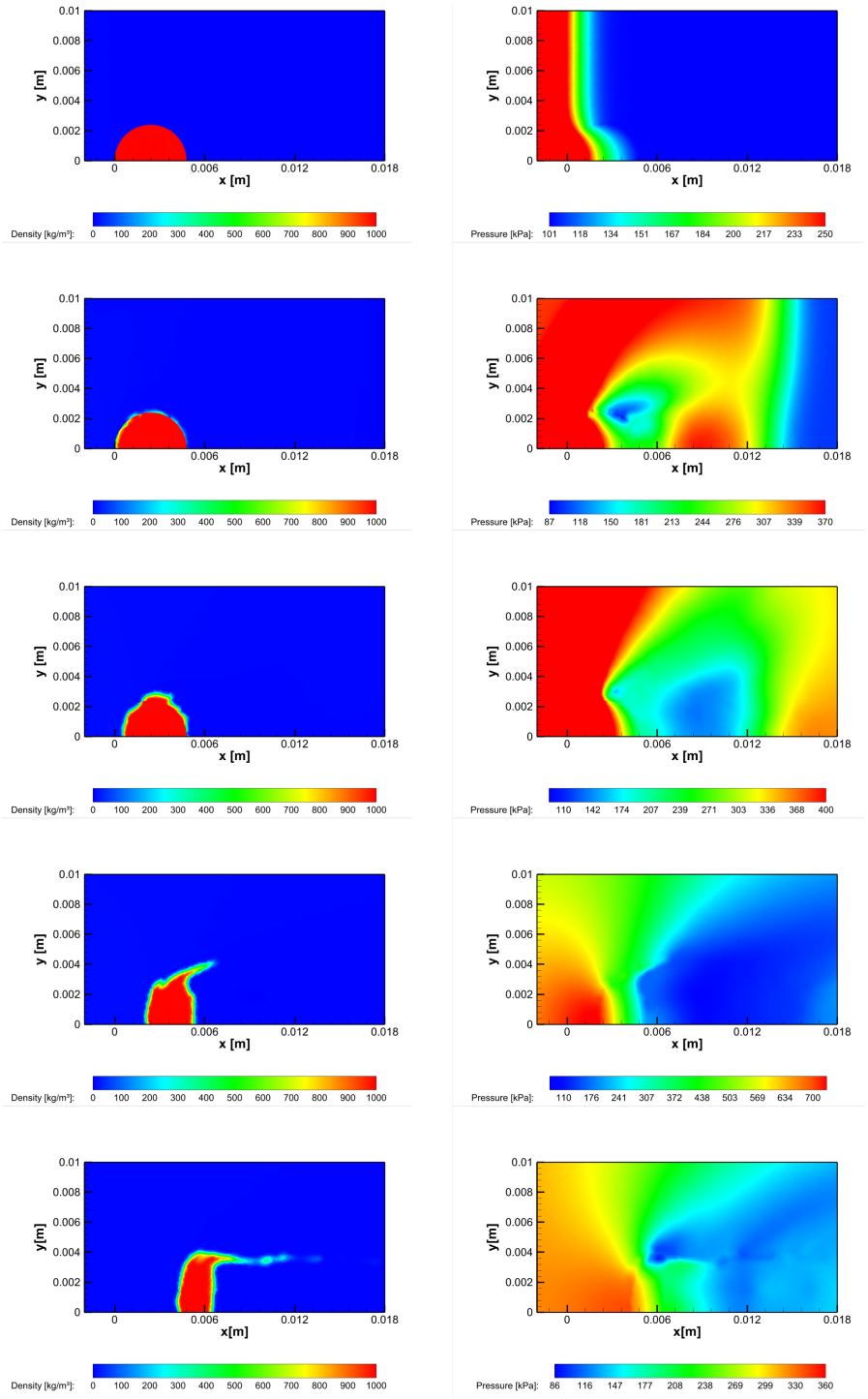

Fig. 3. Contour maps of density (left) and pressure (right) at different time instants corresponding to $t^* = 0.008$, 0.09, 0.24, 0.48, and 0.72 (from top to bottom).

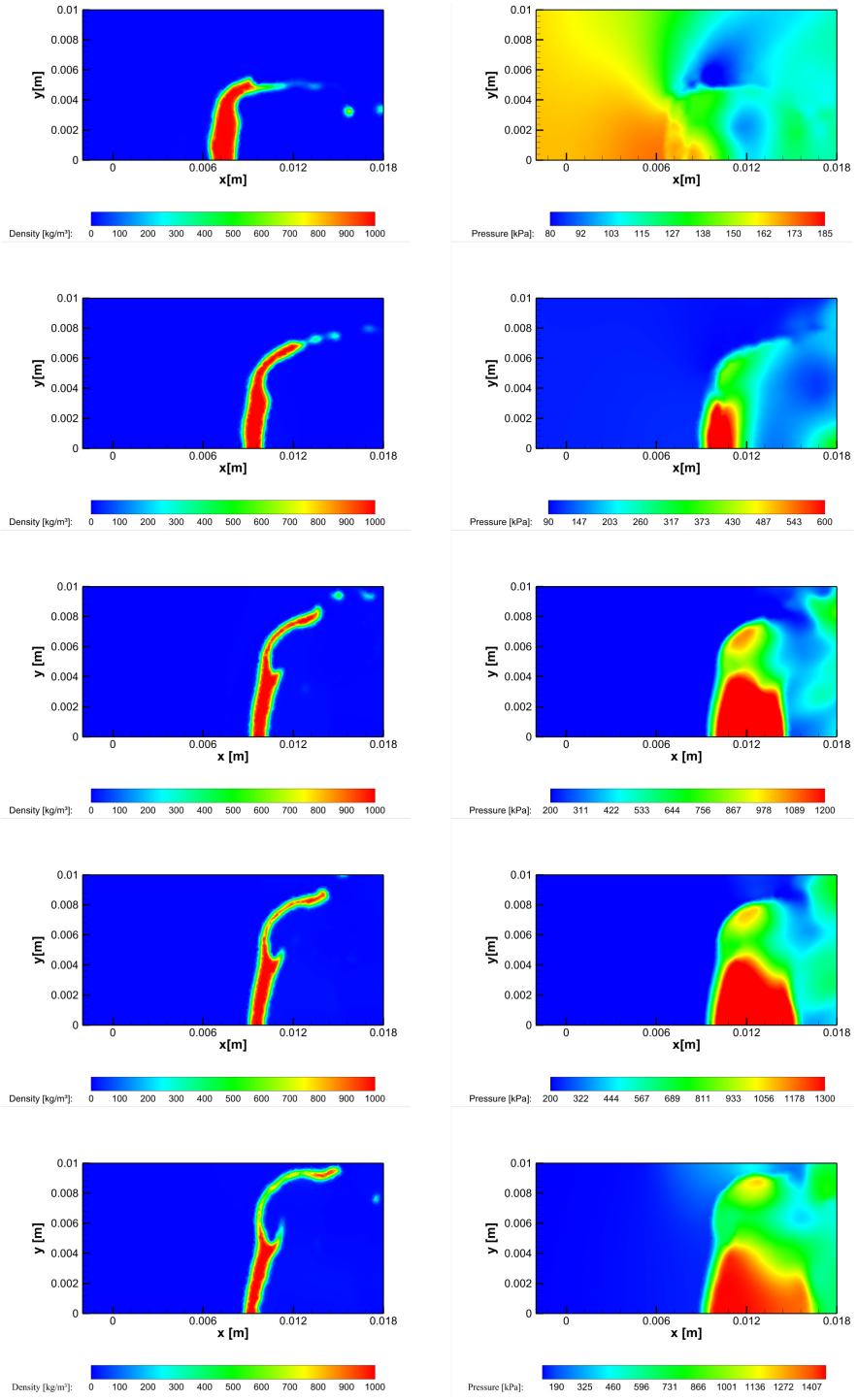

Fig. 4. Contour maps of density (left) and pressure (right) at different time instants corresponding to $t^* = 0.96$, 1.2, 1.32, 1.35, and 1.4 (from top to bottom).

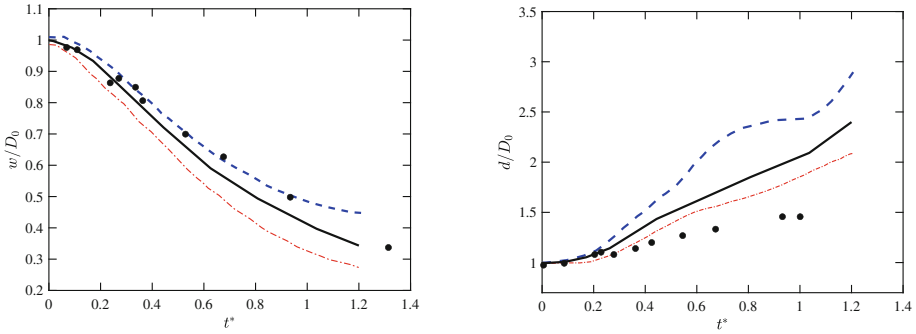

Fig. 5. Time-dependent centerline width (left) and cross-stream length (right) of the water column: present solution (solid line), reference numerical solution [5] (dashed and dashed-dotted lines), and experimental data [11] (symbols).

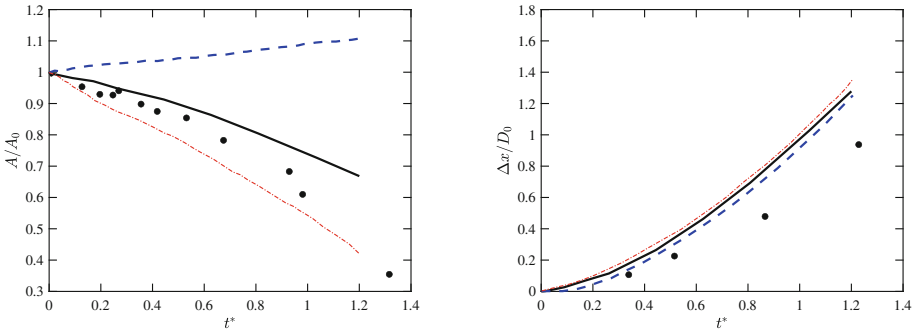

Fig. 6. Time-dependent section area (left) and leading-edge drift (right) of the water column: present solution (solid line), reference numerical solution [5] (dashed and dashed-dotted lines), and experimental data [11] (symbols).

4 Concluding Remarks

The present study has to be intended as the proof-of-concept, namely, the preliminary development of a CFD based prediction tool for the study of the aerodynamic breakup of water droplets in supersonic gas flows. CFD analysis of the early stages of the plane shock wave interaction with a cylindrical water column has been performed. The observed characteristics are in good agreement, both qualitatively and quantitatively, with the reference experimental and numerical results.

There remains the possibility of developing more sophisticated computational models for this particular industrial gas dynamics application, depending on the level of accuracy that is required and the available computational resources. Following [20,21], for example, one possibility could be the use of adaptive methods that make use of the wavelet transform to adjust the numerical grid resolution to the local flow conditions [22–24]. Wavelet-based adaptive URANS modelling

procedures that have been recently developed [25–27] could be explored in this context. Moreover, in order to simulate the appearance of microdroplets, the use of VOF-Lagrangian hybrid methods [28] could be considered, in the framework of either the present industrial CFD solver or the wavelet-based approach [29].

References

1. Liu, N., Wang, Z., Mingbo, S., Wang, H., Wang, B.: Numerical simulation of liquid droplet breakup in supersonic flows. Acta Astronaut. **145**, 116–130 (2018)
2. Villermaux, E.: Fragmentation. Annu. Rev. Fluid Mech. **39**, 419–446 (2017)
3. Wang, Z., Hopfes, T., Giglmaier, M., Adams, N.A.: Effect of Mach number on droplet aerobreakup in shear stripping regime. Exp. Fluids **61**, 193 (2020)
4. Poplavski, S., Minakov, A., Shebeleva, A., Boiko, V.: On the interaction of water droplet with a shock wave: experiment and numerical simulation. Int. J. Multiph. Flow **127**, 103273 (2020)
5. Meng, J.C., Colonius, T.: Numerical simulations of the early stages of high-speed droplet breakup. Shock Waves **25**, 399–414 (2015)
6. Sembian, S., Liverts, M., Tillmark, N., Apazidis, N.: Plane shock wave interaction with a cylindrical water column. Phys. Fluids **28**, 056102 (2016)
7. Rapagnani, D., Buompane, R., Di Leva, A., et al.: A supersonic jet target for the cross section measurement of the 12C(α, γ)16O reaction with the recoil mass separator ERNA. Nucl. Instrum. Meth. Phys. Res. B **407**, 217–221 (2017)
8. Wilcox, D.C.: Turbulence Modeling for CFD, 3rd edn. DCW Industries Inc, La Canada (2006)
9. Hirt, C.W., Nichols, B.D.: Volume of fluid (VOF) method for the dynamics of free boundaries. J. Comput. Phys. **39**, 201–225 (1981)
10. Sod, G.A.: A survey of several finite difference methods for systems of nonlinear hyperbolic conservation laws. J. Comput. Phys. **27**, 1–31 (1978)
11. Igra, D., Takayama, K.: A study of shock wave loading on a cylindrical water column. Technical report, vol. 13, pp. 19–36. Institute of Fluid Science, Tohoku University (2001)
12. Theofanous, T.G., Li, J.G.: On the physics of aerobreakup. Phys. Fluids **20**, 052103 (2008)
13. Theofanous, T.G.: Aerobreakup of Newtonian and viscoelastic liquids. Annu. Rev. Fluid Mech. **43**, 661–690 (2011)
14. Menter, F.R.: Two-equation eddy-viscosity turbulence models for engineering applications. AIAA J. **32**, 1598–1605 (1994)
15. Reina, G.P., De Stefano, G.: Computational evaluation of wind loads on sun-tracking ground-mounted photovoltaic panel arrays. J. Wind Eng. Ind. Aerodyn. **170**, 283–293 (2017)
16. De Stefano, G., Natale, N., Reina, G.P., Piccolo, A.: Computational evaluation of aerodynamic loading on retractable landing-gears. Aerospace **7**, 68 (2020)
17. Natale, N., Salomone, T., De Stefano, G., Piccolo, A.: Computational evaluation of control surfaces aerodynamics for a mid-range commercial aircraft. Aerospace **7**, 139 (2020)
18. Iannelli, P., Denaro, F.M., De Stefano, G.: A deconvolution-based fourth-order finite volume method for incompressible flows on non-uniform grids. Int. J. Numer. Methods Fluids **43**, 431–462 (2003)

19. Rossano, V., De Stefano, G.: Computational evaluation of shock wave interaction with a cylindrical water column. Appl. Sci. **11**, 4934 (2021)
20. Regele, J.D., Vasilyev, O.V.: An adaptive wavelet-collocation method for shock computations. Int. J. Comput. Fluid Dyn. **23**, 503–518 (2009)
21. Hosseinzadeh-Nik, Z., Aslani, M., Owkes, M., Regele, J.D.: Numerical simulation of a shock wave impacting a droplet using the adaptive wavelet-collocation method. In: Proceedings of the ILASS-Americas 28th Annual Conference on Liquid Atomization and Spray Systems, Dearborn, MI, USA, May 2016
22. De Stefano, G., Vasilyev, O.V.: Wavelet-based adaptive large-eddy simulation with explicit filtering. J. Comput. Phys. **238**, 240–254 (2013)
23. De Stefano, G., Brown-Dymkoski, E., Vasilyev, O.V.: Wavelet-based adaptive large-eddy simulation of supersonic channel flow. J. Fluid Mech. **901**, A13 (2020)
24. De Stefano, G., Vasilyev, O.V.: Hierarchical adaptive eddy-capturing approach for modeling and simulation of turbulent flows. Fluids **6**, 83 (2021)
25. De Stefano, G., Vasilyev, O.V., Brown-Dymkoski, E.: Wavelet-based adaptive unsteady Reynolds-averaged turbulence modelling of external flows. J. Fluid Mech. **837**, 765–787 (2018)
26. Ge, X., Vasilyev, O.V., De Stefano, G., Hussaini, M.Y.: Wavelet-based adaptive unsteady Reynolds-averaged Navier-Stokes computations of wall-bounded internal and external compressible turbulent flows. In: Proceedings of the 2018 AIAA Aerospace Sciences Meeting, Kissimmee, FL, USA, January 2018
27. Ge, X., Vasilyev, O.V., De Stefano, G., Hussaini, M.Y.: Wavelet-based adaptive unsteady Reynolds-averaged Navier-Stokes simulations of wall-bounded compressible turbulent flows. AIAA J. **58**, 1529–1549 (2020)
28. Shen, B., Ye, Q., Tiedje, O., Domnick, J.: Simulation of the primary breakup of non-Newtonian liquids at a high-speed rotary bell atomizer for spray painting processes using a VOF-Lagrangian hybrid model. In: Proceedings of the 29th European Conference on Liquid Atomization and Spray Systems, Paris, France, September 2019
29. Nejadmalayeri, A., Vezolainen, A., De Stefano, G., Vasilyev, O.V.: Fully adaptive turbulence simulations based on Lagrangian Spatio-temporally varying wavelet thresholding. J. Fluid Mech. **749**, 794–817 (2014)